Molecular beam studies of weak interactions for openshell systems: The ground and lowest excited states of ArF, KrF, and XeF

Vincenzo Aquilanti, Emilio Luzzatti, Fernando Pirani, and Gian Gualberto Volpi

Citation: The Journal of Chemical Physics **89**, 6165 (1988); doi: 10.1063/1.455433
View online: http://dx.doi.org/10.1063/1.455433
View Table of Contents: http://scitation.aip.org/content/aip/journal/jcp/89/10?ver=pdfcov
Published by the AIP Publishing

Molecular beam studies of weak interactions for open-shell systems: The ground and lowest excited states of ArF, KrF, and XeF

Vincenzo Aquilanti, Emilio Luzzatti,[a] Fernando Pirani, and Gian Gualberto Volpi
Dipartimento di Chimica dell'Università, 06100 Perugia, Italy

(Received 4 April 1988; accepted 25 July 1988)

Absolute integral cross sections for scattering of ground state fluorine atoms by argon, krypton, and xenon have been measured in the thermal velocity range. Information has been obtained on the long range interaction and using a technique for magnetic analysis of substates of F atoms, a characterization is given for the bonding in the ground and the two lowest excited states of these rare gas fluorides. The potentials are represented as a spherical part and an anisotropic component, which have been obtained in an adiabatic decoupling treatment, including also information from other scattering data. Nonadiabatic coupling matrix elements and other general features of these interactions are also presented.

I. INTRODUCTION

Recent active interest in the rare gas halides[1-4] has been motivated both by the peculiar nature of the bonding involved, and by the use of their molecular bands to obtain UV laser action. In particular, for XeF spectroscopic investigations[1(b),1(c)] gave accurately the properties of the ground state near its well, and for KrF[1(a)] some features of the repulsive part of the ground state interaction were obtained; but in general, these interactions appear to be so weak as to be rather elusive to spectroscopic investigations.

For these systems, scattering experiments have been reported by a few groups, using different but in a sense complementary techniques: Differential cross section measurements for fluorine[3] and other halogens[4] scattered by rare gases were analyzed to give ground state interactions and some features of the excited states as well; low energy relative integral cross sections[5] for fluorine scattering by rare gases provide further insight on these interactions; absolute integral cross sections with magnetic analysis of sublevels have been also measured, as communicated previously[6] and fully reported here. All the information available from these sources allow an analysis to be carried out, to provide a characterization of the weak interactions between ground state fluorine atoms and Ar, Kr, and Xe.

Quantum chemistry allows a general description of ground and excited states,[7] which is useful to discuss reactivity and mechanism of laser action. From the analysis of scattering experiments reported in this work, much finer details can be obtained on these weak forces, specifically in the region of the van der Waals wells, thereby allowing a comparative assessment also with the homolog series of rare gas oxides, discussed in the previous paper.[8]

The present analysis exploits recent advances in the quantum mechanical treatment of open shell atom collisions.[9-12] In turn, the interactions obtained in this paper are of interest for the discussion of the polarization, orientation, and alignment cross sections[12] and of transport properties of fluorine atoms in rare gas baths.[13]

Section II outlines those experimental details which are specific to this work. Section III presents the theory of magnetic analysis of atomic sublevels, with particular reference to the angular momentum coupling schemes of interest for fluorine atoms. Section IV summarizes the theoretical framework for the analysis of present and previous[3,5] scattering experiments. The results and their analysis are reported in Sec. V. A discussion of the interactions so obtained is given in Sec. VI. Conclusions follow in Sec. VII.

II. EXPERIMENTAL APPARATUS

The apparatus used to analyze the atomic beam and to perform scattering experiments is the same described earlier in connection with previous absolute integral cross section measurements.[14] Further details are in Ref. 15. Beams of atoms such as H,[14(a)] N,[16] O,[8,17] and F,[6] are produced by 2450 MHz microwave discharge in appropriate gas mixtures, undergo mechanical velocity selection to within $\simeq 5\%$ (FWHM), and are detected by a quadrupole mass filter. The signal is discriminated from background by beam modulation and ion counting.

As previously,[14(b),14(h)] the absolute values of integral cross sections have been obtained by internal calibration based on the direct measurements of the gas flow in the scattering chamber and on the absolute values of the He–Ar integral cross sections reported in Ref. 18.

The magnetic analysis is performed by a Stern–Gerlach magnetic selector,[19] which presents a Rabi configuration, and is inserted along the beam path (see Fig. 1 and Ref. 15). The geometry of the magnet determines the ratio between the average field strength B and its gradient $\partial B/\partial z$ in a direction z normal to the beam path[19(a)]: In our configuration, this ratio is $\simeq 0.25\ \mathrm{cm}^{-1}$. The field strength can be varied by varying the current through the coils up to a maximum value of $B \simeq 6$ kG. As shown in Sec. III, these characteristics of the magnet, together with the geometric features of the apparatus and the finite dimensions of the beam, must be taken into account in the understanding of the experimental results.

[a] On leave from: Istituto di Metodologie Avanzate Inorganiche del Consiglio Nazionale delle Ricerche, Rome, Italy.

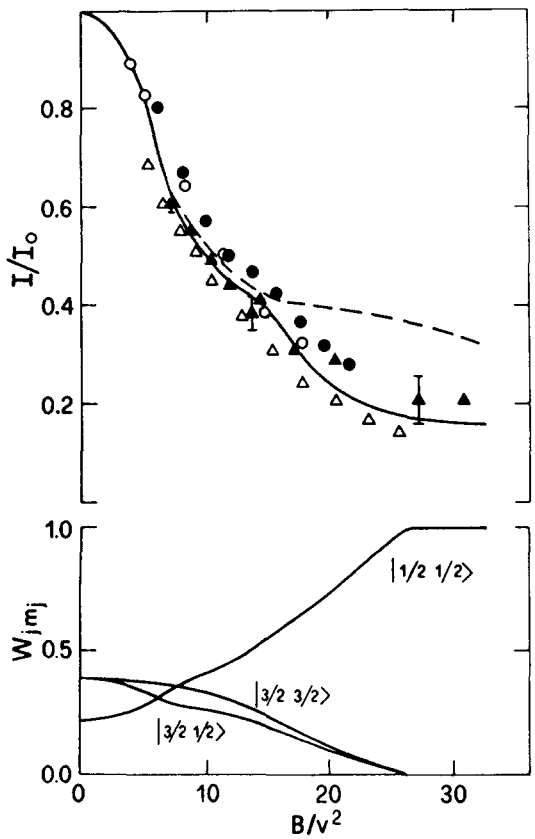

FIG. 1. Fraction I/I_0 of the transmitted beam of F atoms as a function of the reduced parameters B/v^2, where B is the magnetic field strength and v is the velocity of the beam. The abscissa units are in 10^2 G km^{-2} s^2. Black triangles, open triangles, black dots, open dots refer to four different velocities v (1.20, 1.40, 1.60, and 1.75 km s^{-1}, respectively). Dashed line is calculated assuming no nuclear spin decoupling for $j = 3/2$, the full line assuming decoupling (see Sec. III). In the lower panel, the relative weights W_{jm_j} of the $|jm_j\rangle$ states of the F(^2P_j) are shown.

III. COUPLING SCHEMES FOR MAGNETIC ANALYSIS OF ATOMIC SUBLEVELS

When a particle having a mass M and a velocity v interacts with an inhomogeneous magnetic field (with a maximum gradient $\partial B/\partial z \simeq 24$ kG/cm, see Sec. II) for a length ℓ (12 cm in this case), its acceleration a along z is given by by[19(a)]

$$a = \frac{\mu_{km'_k}}{M}\frac{\partial B}{\partial z}. \tag{1}$$

The prime denotes that quantization on the z axis is taken in the direction of the gradient of B and normal to the beam direction, and $\mu_{km'_k}$ is the effective magnetic moment given by

$$\mu_{km'_k} = \mu_0 g_k m'_k. \tag{2}$$

Here, $\mu_0 = 9.27 \times 10^{-28}$ J/G is the Bohr magneton, g_k is the Landè factor depending on the quantum number k which adequately describes the atomic states in the magnet (see below) and m'_k is its projection along z. The paramagnetic particle undergoes, at a distance $\mathscr{L}$ from the magnet, a deflection δ along the z direction which is given by two contributions: The first proportional to $\ell/2$ and due to an approximate uniformly accelerated motion within the magnet[20]; the second proportional to $\mathscr{L}$ and due to a uniform rectilinear motion outside the magnet. Therefore,

$$\delta = \frac{\mu_{km'_k}}{Mv^2}\left(\frac{\partial B}{\partial z}\right)\ell\left(\frac{\ell}{2} + \mathscr{L}\right). \tag{3}$$

For the present experiments the distance $\mathscr{L}$ between the exit of the magnet and the entrance slit of the detector is $\simeq 50$ cm.

The effects of the magnetic analysis carried out on a beam of paramagnetic atoms can be exploited not only to extract information on the atomic sublevels involved, but also to change their relative population in the fraction of the beam transmitted to the detector; this is due to the fact that the atomic sublevels interact differently with the field, according to their magnetic moments. Therefore, scattering experiments performed at different values of the magnetic field B allow to obtain unique information on the anisotropic interactions of open shell atomic species.[19]

For an atom with a nuclear spin quantum number $i \neq 0$ and with an electron angular momentum quantum number L and a spin S, besides $j \neq 0$ ($\mathbf{j} = \mathbf{L} + \mathbf{S}$), also the possible coupling of j and i has to be taken into account. Therefore, the good quantum number k to be used in the above formulas (1)–(3), can be either f ($\mathbf{f} = \mathbf{j} + \mathbf{i}$), or j, or L and S quantized independently. In order to decide which one is the appropriate quantum number for each atomic state, one has to compare the value of the product $\mu_0 B$ with the fine $\Delta_{j,j+1}$ and hyperfine structure intervals $\Delta_{f,f+1}$. If $\mu_0 B \lesssim \Delta_{f,f+1}$, the good quantum number k is f; if $\Delta_{f,f+1} < \mu_0 B < \Delta_{j,j+1}$, the appropriate quantum number is j (Back–Goudsmit effect), if $\mu_0 B \gtrsim \Delta_{j,j+1}$, the $\mu_{km'_k}$ value is determined by L and S independently quantized (Paschen–Back effect).

In the case of a beam of fluorine atoms in the lowest ^2P electronic state, the fine structure components $j = 3/2$ and $j = 1/2$ must be taken into account. Under the present conditions (beam temperature $\simeq 10^3$ K, as estimated from the measured Maxwell–Boltzmann velocity distribution), F atoms are for 78% in the ground $^2P_{3/2}$ state, and 22% in the $^2P_{1/2}$ state, separated by the fine structure splitting $\Delta_{1/2,3/2} = 404$ cm^{-1}. On the other hand, the ^{19}F nucleus has $i = 1/2$, and the possible coupling of j and i has to be considered. While the magnetic field obtainable in our experiments cannot achieve Paschen–Back conditions (decoupling of j in L and S), hyperfine effects play a different role for $j = 3/2$ and $j = 1/2$ states. The hyperfine structure interval for $j = 3/2$ is 6.706 10^{-2} cm^{-1},[21] sufficiently small to allow decoupling of j and i at the highest fields. However, for the $j = 1/2$ atoms, which have a very large hyperfine structure interval (3.417 10^{-1} cm^{-1}),[21] j and i remain coupled to give f as a good quantum number.

This treatment of the behavior of a fluorine atom beam under the present experimental conditions allows us to determine the relative weight $W_{km'_k}$ of each $|km'_k\rangle$ state of F atoms in the beam as a function of the magnetic field strength B at a given velocity v.

In Fig. 1 the beam transmittance I/I_0, where I is the beam intensity with the field applied and I_0 is the intensity at

zero field, measured at four different velocities, is reported as a function of the quantity B/v^2. The use of the function B/v^2 makes the plot of the transmittance independent from the beam velocity v. The figure also shows the transmittance I/I_0 calculated using the formula

$$I/I_0 = \sum_{k,m'_k} W^0_{km'_k} F_{km'_k}(B/v^2), \tag{4}$$

where $W^0_{km'_k}$ is the normalized weight at zero field of each $|km'_k\rangle$ state (for an effusive beam it depends essentially on the temperature in the source, see above), and $F_{km'_k}(B/v^2)$, a function ranging between 0 and 1, is the transmission for the atomic state $|km'_k\rangle$: it depends on the effective magnetic moment $\mu_{km'_k}$, and is obtained from Eq. (3) for the deflection δ introducing the geometric features of the apparatus and the finite dimensions of the beam (the effect of the latter is to effectively smooth out the transmission calculated for an infinitely narrow beam).

Calculations have been performed using either (i) j as a good quantum number for the ground state $j = 3/2$, and $\not{j}$ for the $j = 1/2$ state; or (ii) $\not{j}$ as appropriate for both levels. The effective magnetic moments for each sublevel are reported in Table I for the different coupling schemes considered. From the figure it is evident that at high magnetic fields only coupling scheme (i) correctly describes the experimental results, while at low fields the transmission curves calculated from both (i) and (ii) show a similar behavior. The following conclusion can be drawn: When the magnetic field is sufficiently high ($B > 1.5$ kG) a complete Back–Goudsmit effect (decoupling of j from i) occurs for the ground state $j = 3/2$. On the other hand, at low values of B ($B \lesssim 1.5$ kG), where only an incipient Back–Goudsmit effect is present, the atoms which are deflected are essentially those with maximum $\mu_{km'_k}$ (which have a value of $2\mu_0$ for both coupling schemes): Therefore both calculations reproduce the experimental data (Fig. 1) at low fields.

The relative weights $W_{km'_k}$ in the transmitted beam can be connected to the transmittance I/I_0 by normalizing each term of the sum in Eq. (4):

$$W_{km'_k} = \frac{W^0_{km'_k} F_{km'_k}(B/v^2)}{I/I_0}. \tag{5}$$

TABLE I. Effective magnetic moments in alternative coupling schemes.[a]

Coupling scheme	Magnetic moment
$\|(ji)\not{j}m'_{\not{j}}\rangle$	$\mu_{\not{j}m'_{\not{j}}}$
$\|(3/2\ 1/2)\ 2 \pm 2\rangle$	$2\mu_0$
$\|(3/2\ 1/2)\ 2 \pm 1\rangle$	μ_0
$\|(3/2\ 1/2)\ 1 \pm 1\rangle$	$(5/3)\mu_0$
$\|(1/2\ 1/2)\ 1 \pm 1\rangle$	$(1/3)\mu_0$
$\|(1/2\ 1/2)\ 0\ 0\rangle$	0
$\|jm'_j\rangle$	$\mu_{jm'_j}$
$\|3/2 \pm 3/2\rangle$	$2\mu_0$
$\|3/2 \pm 1/2\rangle$	$(2/3)\mu_0$
$\|1/2 \pm 1/2\rangle$	$(1/3)\mu_0$

[a] See Eq. (2). Landè factors g_k are from Ref. 22.

In order to determine the weights of atomic magnetic sublevels appropriate for the analysis of scattering experiments, we have to take into account that the laboratory quantization axis, defined by the B direction z, is perpendicular to the direction of the beam (it is this direction which asymptotically coincides with the interatomic axis). To obtain the appropriate weights in the collision frame W_{km_k} (quantization axis along the relative velocity direction), it is necessary to perform a rotation by $\pi/2$ of the reference axis:

$$W_{km_k} = \sum_{m'_k} (d^{(k)}_{m_k m'_k}(\pi/2))^2 W_{km'_k}. \tag{6}$$

The quantities $d_{m_k m'_k}(\pi/2)$ are the elements of the k th-rank rotation matrix.[23] The W_{km_k} weights vary as a function of B/v^2 as shown in Fig. 1 and are labeled in terms of j and m_j because the electric field along the interatomic axis, even at large distances, is strong enough to decouple j and i.

In our apparatus, as a precaution to let the atoms remain oriented from the collision zone to the strong inhomogeneous magnetic field which allows the selection, a weak field which is homogeneous across the beam direction has been applied by connecting at the magnetic expansions two bars of permeable material: These bars extend to embrace the scattering chamber, where the magnetic field was measured to be between 10 and 50 G. This small field should be sufficient to avoid the so-called Majorana flops,[19(a)] i.e., the spontaneous transitions between the components of the atomic magnetic sublevels, induced by rapid variations in the direction of the magnetic field. This experimental detail is very important in the study of the interaction between oxygen atoms $O(^3P)$ with rare gases, where the magnetic analysis allows us to study the scattering of particles having $m'_j = 0$.[8] For atoms having $i \neq 0$ the degree of polarization is generally reduced because of possible recouplings between j and i in the region between the magnetic selector and the scattering chamber. To avoid loss of polarization one should use magnetic fields strong enough to decouple j and i along the whole beam path between scattering chamber and magnetic selector. However, for the fluorine atoms produced in our apparatus, neither the Majorana flops nor the depolarization for recoupling of j and i are very important, because scattering measurements at high B/v^2 values probe mainly the interaction of the $j = 1/2$ state (see Fig. 1), which, as will be seen in detail below, correlates with only a single adiabatic potential energy curve.

IV. THEORETICAL FRAMEWORK

The theory needed to interpret the scattering results of open shell atoms has been given elsewhere[9–11,24,25] and reviewed, in the $O(^3P)$ case, in the previous paper.[8] A proper label for scattering states is $|j\Omega\rangle$, where j is the atomic total angular momentum and Ω is the absolute value of its projection along the interatomic axis. At large interatomic distances Ω tends to the atomic sublevel projection $|m_j|$. For the analysis of the present data it is convenient to define three effective adiabatic potential energy curves $V_{|j\Omega\rangle}$[9–11,24,25] correlating with the different $|jm_j\rangle$ states of F atom ($\Omega = |m_j|$) as follows:

$$V_{|3/2\,1/2\rangle} = V_0 + \tfrac{1}{10} V_2 + \tfrac{1}{2}\Delta - \tfrac{1}{2}(\tfrac{9}{25} V_2^2 + \Delta^2 - \tfrac{2}{5} V_2\Delta)^{1/2},$$
$$V_{|3/2\,3/2\rangle} = V_0 - \tfrac{1}{5} V_2, \qquad (7)$$
$$V_{|1/2\,1/2\rangle} = V_0 + \tfrac{1}{10} V_2 + \tfrac{1}{2}\Delta + \tfrac{1}{2}(\tfrac{9}{25} V_2^2 + \Delta^2 - \tfrac{2}{5} V_2\Delta)^{1/2},$$

where Δ is the spin–orbit constant equal to 404 cm^{-1} = 80.2 meV for fluorine.

The V_0, spherical component, and V_2, anisotropic component, are related[10,26] to the perhaps more familiar V_Σ and V_Π electrostatic interactions by

$$V_0 = \frac{2V_\Pi + V_\Sigma}{3}, \quad V_2 = \tfrac{5}{3}(V_\Sigma - V_\Pi). \qquad (8)$$

Σ and Π stand for $\Lambda = 0$ and $\Lambda = 1$, respectively, where the quantum number Λ is the projection of the electronic angular momentum L on the interatomic axis.

The coupling between these potential energy curves is represented by a matrix **P** whose elements are

$$P_{j\Omega, j'\Omega} = \langle j\Omega | \frac{d}{dR} | j'\Omega \rangle. \qquad (9)$$

The coupling is effective only between states having the same Ω quantum number. In the present case only one element of the **P** matrix is different from zero: it couples the two $\Omega = 1/2$ states, and can be shown to be given by

$$\langle 3/2\ 1/2 | \frac{d}{dR} | 1/2\ 1/2 \rangle = \frac{10\sqrt{2}}{9\beta^2 - 10\beta + 25} \frac{d\beta}{dR}, \quad \text{where } \beta \equiv V_2/\Delta. \qquad (10)$$

When the contribution from these off diagonal elements can be neglected (as in this case, see below), the integral cross sections will be given by a weighted sum of the cross sections $Q_{j\Omega}(v)$ for scattering by the potentials $V_{|j\Omega\rangle}$:

$$Q(v) = \sum_{j,\Omega} W_{j\Omega} Q_{j\Omega}(v). \qquad (11)$$

In the present case the weights $W_{j\Omega}$ are known from Sec. III and depend on the magnetic field strength (Fig. 1).

A proper extension of this equation will be used in the following for the analysis of differential cross sections.[3]

V. RESULTS AND DATA ANALYSIS

The absolute integral cross sections Q for F–Ar, Kr, and Xe collisions, measured as a function of the beam velocity v, are reported in Figs. 2, 3, and 4. As usual the cross sections have been plotted as $Qv^{2/5}$ to show the glory structure.[14] The measurements have been performed, for all systems, at zero

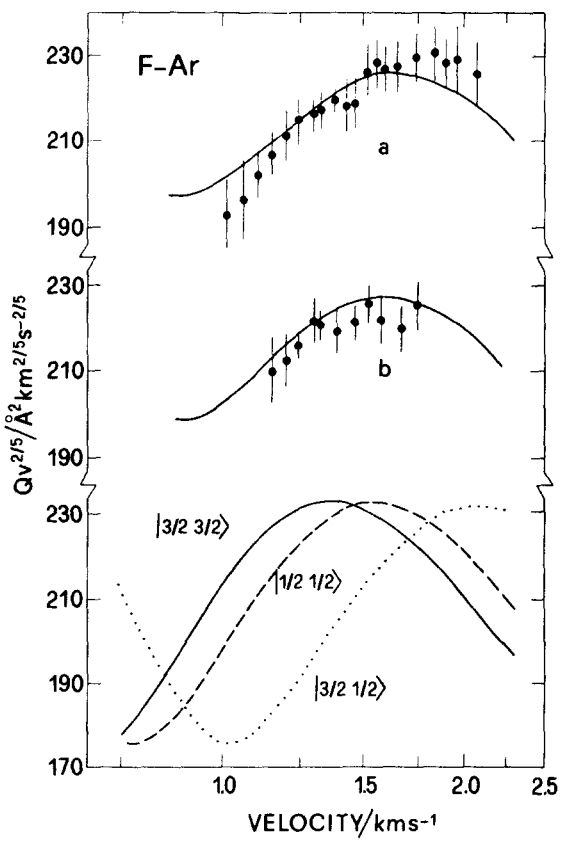

FIG. 2. Absolute integral cross sections for the F–Ar system as a function of the velocity v: (a) at zero field; (b) at $B/v^2 = 9\times10^2$ G km^{-2} s^2 (see also Fig. 1 and Table II). The calculated cross sections from the single adiabatic potential energy curves $V_{|j\Omega\rangle}$ [see Eq. (7)] are shown at the bottom: they are combined according to Eq. (11) with weights as in Table II.

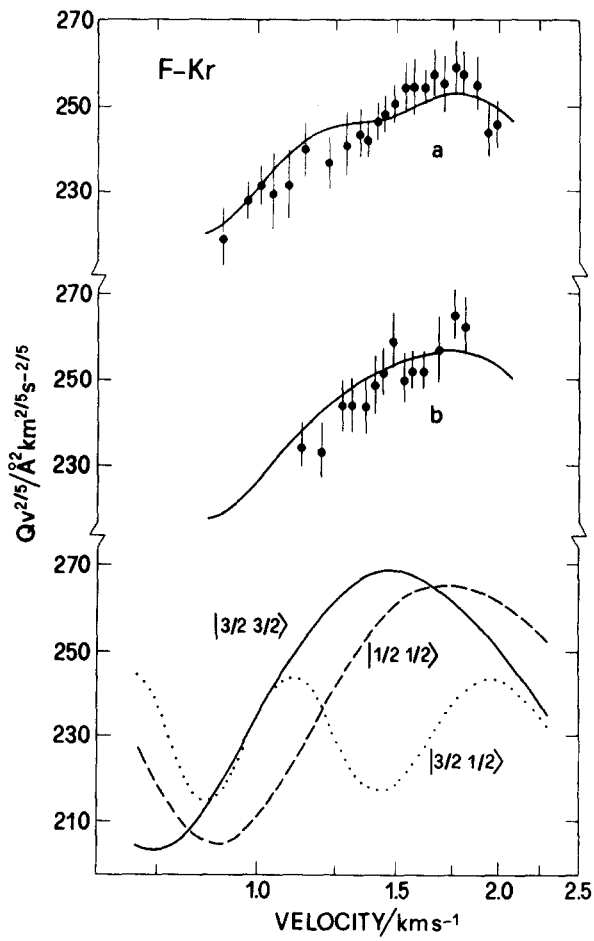

FIG. 3. Absolute integral cross sections for the F–Kr system as a function of the velocity v: (a) at zero field; (b) at $B/v^2 = 9\times10^2$ G km^{-2} s^2 (see also Fig. 1 and Table II). As for Fig. 2 the calculated cross sections from the single adiabatic potential energy curves $V_{|j\Omega\rangle}$ are shown at the bottom.

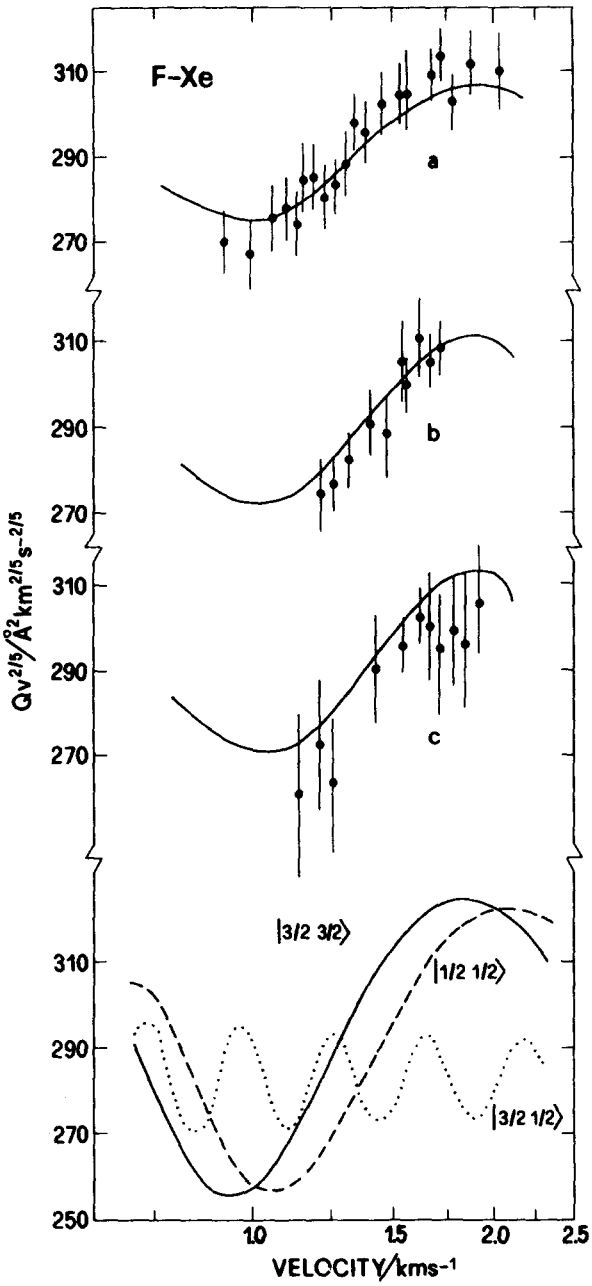

FIG. 4. Absolute integral cross sections for the F–Xe system as a function of the velocity v: (a) at zero field; (b) at $B/v^2 = 9$; (c) at $B/v^2 = 17$ (the units are in 10^2 G km^{-2} s^2, see also Fig. 1 and Table II). As for Fig. 2, the calculated cross sections from the single adiabatic potential energy curves $V_{|J\Omega\rangle}$ are shown at the bottom.

and at finite values of the magnetic field. Table II lists the weights of the magnetic sublevels for the conditions which apply to present measurements of F atom scattering. They have been obtained according to Sec. III.

In addition to our data, other scattering properties are available, in particular relative integral cross sections at low velocities[5] and differential cross sections.[3] In a previous analysis of the F–Xe system,[6] we analyzed our data together with some features of the emission spectrum.[1(b),1(c)] All scattering properties and the general features of the emission

TABLE II. Fraction of transmitted F atom beam and its composition.

B/v^2 (10^2 G km^{-2} s^2)	Fraction of transmitted beam I/I_0	W_{jm_j}[a]		
		$\|3/2\ 3/2\rangle$	$\|3/2\ 1/2\rangle$	$\|1/2\ 1/2\rangle$
0	1.00	0.39	0.39	0.22
9	0.50	0.31	0.25	0.44
17	0.33	0.23	0.18	0.59

[a] Atomic projections m_j refer to the beam direction. Under present experimental conditions they adiabatically correlate with the projections Ω on the interatomic axis.

spectra[1] are taken into account in the present analysis for all three systems.

Integral cross sections have been calculated from Eq. (11) and the differential cross sections by combining in a similar way those from scattering from each potential in Eq. (7). In the case of the present scattering data the $W_{j\Omega}$ are experimentally determined (Sec. III, Table II), while in the other cases[3,5] they have to be estimated from the nozzle source temperature. Individual integral cross sections $Q_{j\Omega}(v)$ have been obtained by the $V_{|j\Omega\rangle}$ potentials using an accurate semiclassical procedure given elsewhere[27] while differential cross sections have been obtained computing JWKB phase shifts for scattering by the same potentials. These potentials are produced from Eqs. (7) once V_0 and V_2 are specified.

Since the scattering data analyzed in this work come from different sources which provides several pieces of information, we have used the flexible ESMSV (exponential, switching, Morse, switching, van der Waals) parametrization for V_0,[28] scaling for the location R_m and the depth ϵ of the well:

$$x = R/R_m; \quad f(x) = V_0(R)/\epsilon; \tag{12a}$$

exponential:

$$f(x) = A(x) = Ae^{-\alpha(x-1)}, \quad x \leqslant x_1; \tag{12b}$$

switching from exponential to Morse:

$$\text{(i)}\ f(x) = S(x)A(x) + [1 - S(x)]M(x), \quad x_1 < x < x_2; \tag{12c}$$

Morse:

$$f(x) = M(x) = e^{-2\beta(x-1)} - 2e^{-\beta(x-1)}, \quad x_2 \leqslant x \leqslant x_3; \tag{12d}$$

switching from Morse to van der Waals:

$$\text{(ii)}\ f(x) = S(x)M(x) + [1 - S(x)]W(x), \quad x_3 < x < x_4; \tag{12e}$$

van der Waals:

$$f(x) = W(x) = -\left(\frac{C_0}{\epsilon R_m^6}\right)x^{-6}, \quad x_4 \leqslant x, \tag{12f}$$

where C_0 is the long range R^{-6} constant. Switching functions were taken as

$$S(x) = \frac{1}{2}\left[\cos\frac{\pi(x-x_a)}{(x_b-x_a)}+1\right] \quad \begin{matrix}\text{in (i): } x_a = x_1 \\ x_b = x_2 \\ \text{in (ii): } x_a = x_3 \\ x_b = x_4\end{matrix} \tag{12g}$$

For the anisotropic interaction $V_2(R) = 5(V_\Sigma - V_\Pi)/3$ simple quantum chemical arguments suggest that at short range, where it decays exponentially, $V_\Sigma < V_\Pi$. On the other hand, at long range, $V_\Sigma > V_\Pi$ and $V_2(R)$ is mainly due to the anisotropy in the polarizability of the fluorine atom.[29] Therefore, the following, Buckingham type, model for V_2 has been used:

$$V_2(R) = -A_2 e^{-\alpha_2 R} + C_2/R^6. \tag{13}$$

The C_0 constant in Eq. (12f) has been obtained from the absolute value of the cross sections as measured in our experiments; x_3 and x_4 are fixed at 1.1 and 1.5 values, respectively, for all three systems. The C_2/C_0 ratio was estimated from the relative value of the anisotropy polarizability of fluorine atom[29]: Our experiments and all the features discussed in the following are rather insensitive to it. The other parameters have been varied to obtain the best agreement with the experimental data. In particular, the short range parts of V_0 and V_2 terms determine the features of the repulsive and well regions of the ground state $V_{|3/2\,1/2\rangle}$, while the intermediate parts of V_0 and V_2 determine the well depth properties of the excited states $V_{|3/2\,3/2\rangle}$, $V_{|1/2\,1/2\rangle}$, and the attractive region of $V_{|3/2\,1/2\rangle}$.

In the case of the F–Ar system all scattering properties (the present ones and those in Refs. 3 and 5), are sensitive to the three effective potentials $V_{|j\Omega\rangle}$, Eq. (7). Similarly, in the case of the F–Kr system, all these scattering properties give information on the three effective potentials $V_{|j\Omega\rangle}$: In addition, the general features of the repulsive region of $V_{|3/2\,1/2\rangle}$ have been estimated to agree with the spectroscopic data[1(a)]. For the F–Xe system the present absolute integral cross sections (see also Ref. 6) fix the value of the potentials at long range and give information only on the well characteristics of $V_{|3/2\,3/2\rangle}$ and $V_{|1/2\,1/2\rangle}$ because any contribution from the ground state $V_{|3/2\,1/2\rangle}$ is experimentally washed out by the thermal motion of Xe. The other scattering data[3,5] provide

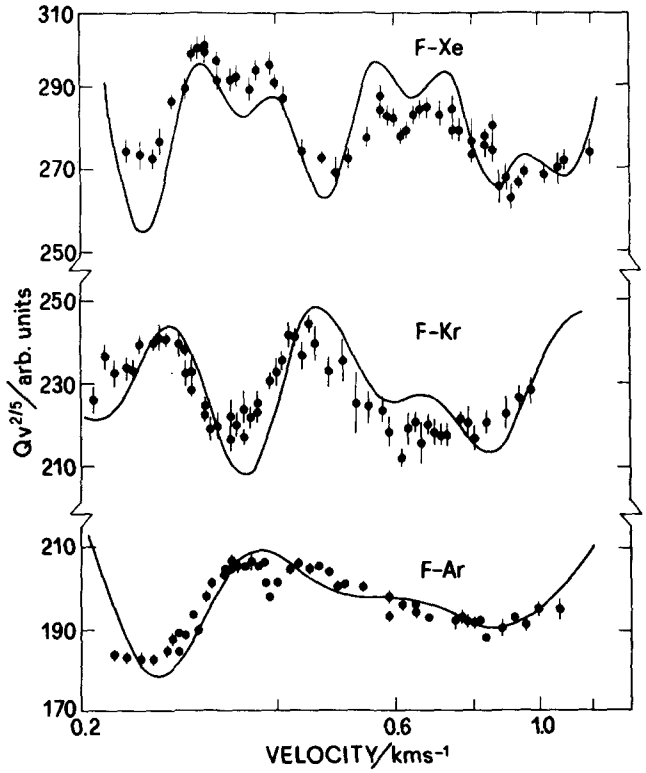

FIG. 5. Integral cross sections for F–Ar, Kr, and Xe collisions measured as a function of the velocity v obtained in Göttingen (Ref. 5), and given in arbitrary units, are compared with curves obtained by scattering calculations from potentials derived in this work (see the text). Weights for Eq. (11) have been estimated assuming Boltzmann population of levels in the nozzle. Numbers on the ordinate scale, in units as in Figs. 2–4, are absolute values from calculations.

TABLE III. Potential parameters for the F(^2P)–Ar, Kr, and Xe systems.

Spherical interaction $V_0(R)$	F–Ar	F–Kr	F–Xe
ϵ/meV	6.8	7.2	8.1
R_m/Å	3.50	3.65	3.78
β	5.8	5.3	5.91
A	0.3350	0.4900	0.2221
α	13.5	14.0	16.0
C_0/(meV Å^6)	1.998×10^4	2.840×10^4	4.744×10^4
x_1	0.7000	0.6750	0.5000
x_2	0.8780	0.8100	0.8700
x_3	1.1000	1.1000	1.1000
x_4	1.5000	1.5000	1.5000
Anisotropic interaction $V_2(R)$	**F–Ar**	**F–Kr**	**F–Xe**
A_2/meV	1.5605×10^6	4.4320×10^6	1.3265×10^7
α_2/Å^{-1}	3.5000	3.5000	3.7000
C_2/(meV Å^6)	2.278×10^3	3.246×10^3	5.660×10^3

further information on the well characteristics for all three effective interaction potentials. For this system the emission spectrum[1(b)] presents a 3500 Å band which is sensitive to the features of the ground state around the equilibrium distance[1(c)]: This spectrum is the main source for the characterization of this very strong interaction.[6]

The calculated integral cross sections have been convoluted in the laboratory system for the direct comparison with the present experimental absolute cross sections, using the procedure described in Ref. 30. A direct comparison in the center of mass system has been made with the Göttingen integral relative cross sections.[5] The calculated differential cross sections are convoluted in the laboratory system[31] for a comparison with the experiments.[3]

The potential parameters so obtained are reported in Table III while the calculated cross sections are compared with those measured in Figs. 2–6. In view of the uncertainties associated mainly with the estimates of magnetic sublevels population in the analysis of Berkeley[3] and Göttingen[5] experiments, the overall description of all scattering properties by present analysis appears to be satisfactory.

VI. DISCUSSION

The interaction between fluorine atoms with the rare gases is anisotropic and in the adiabatic decoupling scheme which describes low energy scattering experiments it is given by three effective potential energy curves which correlate with the different atomic sublevels of $F(^2P_j)$: The present analysis gives these curves for the F–Ar, Kr, and Xe systems which are reported in Figs. 7–9. They are obtained using Eq. (7) with the V_0 and V_2 parameters listed in Table III. This analysis should be more accurate than a previous one,[3] which had available only spectroscopic and differential cross section data and included the dynamical approximation of degenerate excited states.

In Table IV some characteristic parameters for all curves are also presented. It is interesting to note that the well depth ϵ of the ground state increases from F–Ar to F–Xe while its location R_m changes in the opposite way; the well depths of the two excited states change slightly while

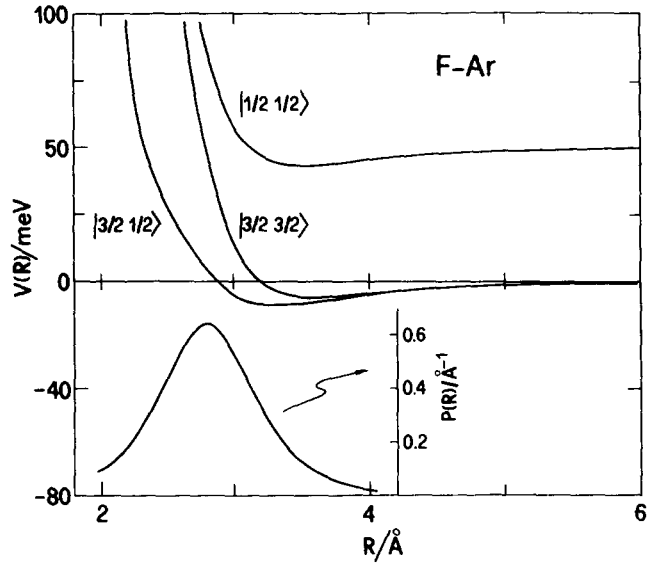

FIG. 7. Adiabatic potential energy curves $V_{|J\Omega\rangle}$ for the F–Ar system. Also shown in the figure is the nonadiabatic coupling matrix element P between the $|3/2\ 1/2\rangle$ and $|1/2\ 1/2\rangle$ states.

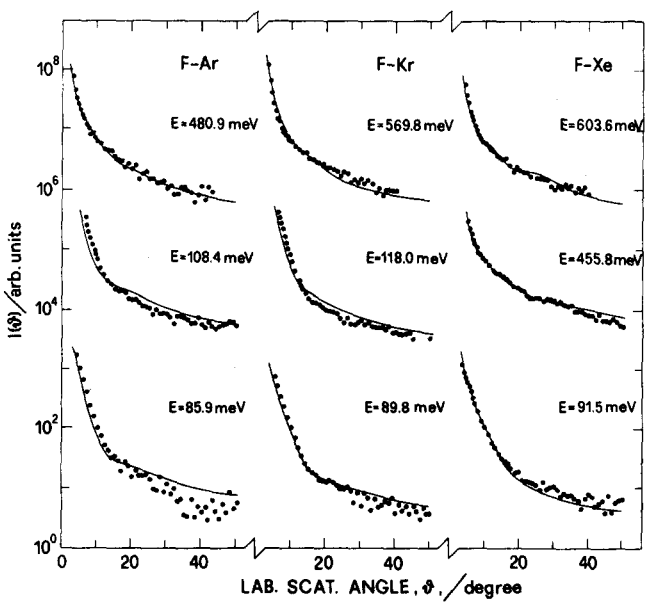

FIG. 6. Total differential cross sections for F–Ar, Kr, and Xe collisions measured at three different energies in Berkeley (Ref. 3). Curves represent scattering calculations from potentials obtained in this work (see the text). The relative weights from Eq. (11) have been estimated assuming Boltzmann population of levels in the nozzle.

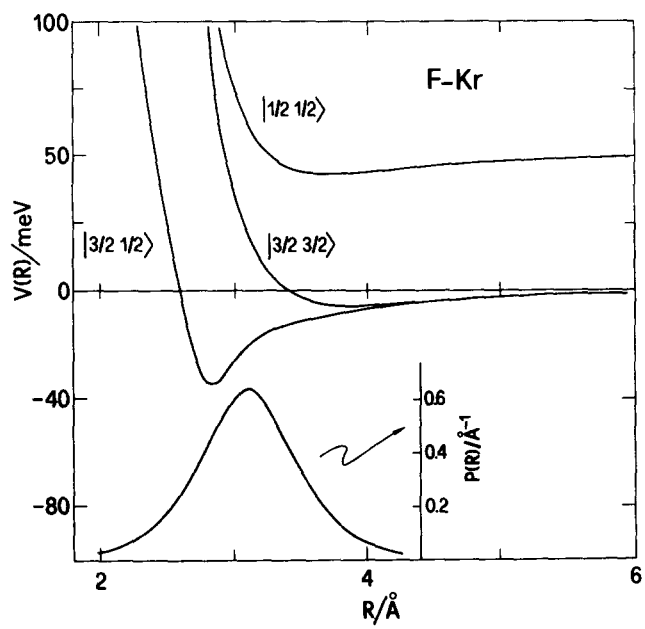

FIG. 8. Adiabatic potential energy curves $V_{|J\Omega\rangle}$ for the F–Kr system. Also shown in the figure is the nonadiabatic coupling matrix element P between the $|3/2\ 1/2\rangle$ and $|1/2\ 1/2\rangle$ states.

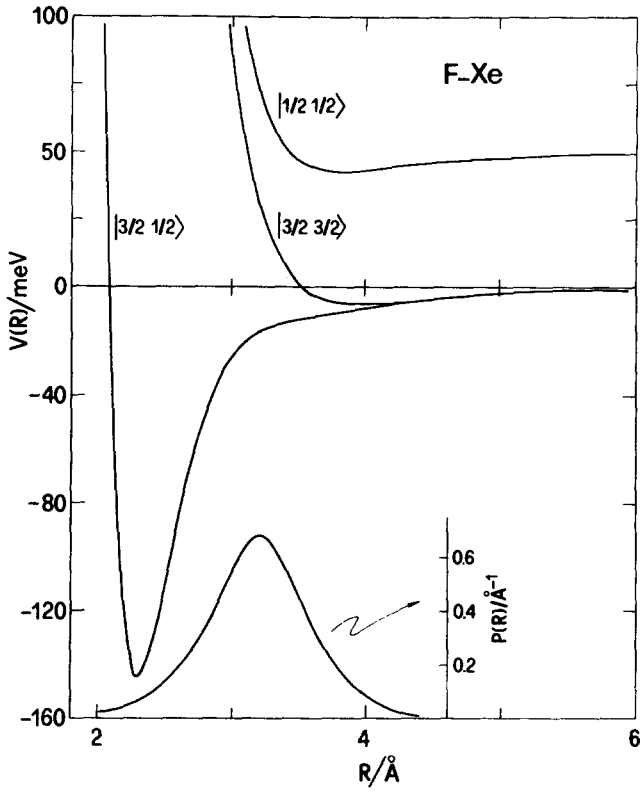

FIG. 9. Adiabatic potential energy curves $V_{|J\Omega\rangle}$ for the F–Xe system. Also shown in the figure is the nonadiabatic coupling matrix element P between the $|3/2\ 1/2\rangle$ and $|1/2\ 1/2\rangle$ states.

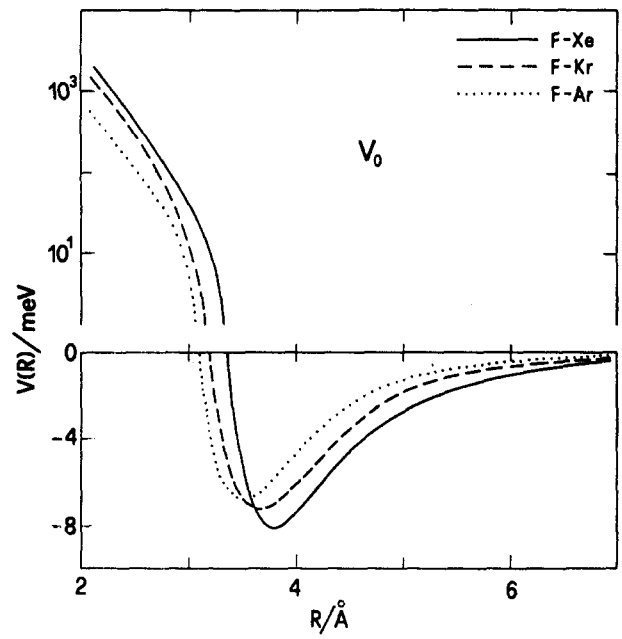

FIG. 10. Spherical interactions V_0 as a function of interatomic distances.

their locations increase regularly going from F–Ar to F–Xe. For a better understanding of these results, a direct comparison of V_0 and V_2 and the related interactions V_Σ and V_Π is reported in Figs. 10–13 for the three systems. For the V_0 term (Fig. 10) both the well depths and their locations increase from F–Ar to F–Xe, in agreement with the trend which can be predicted from considerations of the polarizabilities[32] of the rare gas atoms. The interaction anisotropy V_2 increases from Ar to Xe: The repulsive wall (Fig. 11) shifts at larger distances and this can be attributed to an increasing ionic contribution to the interaction due to a lower ionization potential in going from Ar to Xe. As a consequence, while the V_Π interactions present rather similar (Fig. 13) well depths and shapes, the V_Σ interactions (Fig. 12) vary in a more pronounced way because they are more sensitive to the anisotropy: This is clearly seen by considering their reduced forms, obtained normalizing the potential at the depths and locations of their minima, as, e.g., in Eq. (12a) (see Fig. 12). This is of interest to understand the nature of these interactions, as will be further discussed below.

TABLE IV. Some characteristic features of ArF, KrF, and XeF interactions.[a]

		F–Ar	F–Kr	F–Xe
	ϵ	6.8	7.2	8.1
V_0	R_m	3.50	3.65	3.78
	σ	3.08	3.17	3.34
	ϵ	0.11	0.11	0.24
V_2	R_m	4.88	5.21	5.02
	σ	4.41	4.72	4.56
	ϵ	12.0	47.3	161.8
V_Σ	R_m	3.12	2.83	2.31
	σ	2.73	2.55	2.07
	ϵ	5.8	5.7	6.8
V_Π	R_m	3.61	3.85	3.93
	σ	3.20	3.39	3.50
	ϵ	8.7	34.4	145.4
$V_{\|3/2\ 1/2\rangle}$	R_m	3.31	2.84	2.31
	σ	2.89	2.60	2.08
	ϵ	6.7	7.1	8.0
$V_{\|1/2\ 1/2\rangle}$	R_m	3.51	3.69	3.80
	σ	3.11	3.25	3.39

[a] Parameters for $V_{|3/2\ 3/2\rangle}$ are the same as for V_Π [see Eqs. (7)]. Well depths ϵ, their positions R_m, and zeros of the potentials σ are in meV and Å, respectively. Estimated uncertainties are about 10% for ϵ and 2% for R_m and σ except for the ground state of F–Xe $V_{|3/2\ 1/2\rangle}$ where they are 2% for ϵ and 1% for R_m and σ.

An important indication in this direction is given by the nonadiabatic coupling matrix elements $P(R)$ obtained from Eq. (10) and reported in the lower panels of Figs. 7–9. The $P(R)$ functions for all three systems present a maximum at a distance, where V_2 is of the order of the fine structure splitting Δ, and therefore where the transition between an atomic coupling scheme [Hund's case (c)] at long range and a molecular coupling scheme [Hund's case (a)] at short range occurs. Case (c)[10,11,24] defines as good quantum numbers j and Ω to describe the interaction, while case (a) defines as good quantum numbers Λ and Ω (Λ being the projection of L along the interatomic axis). From the position of the $P(R)$ maximum it is possible to deduce that while the well depth of the ground state of F–Ar is completely described by Hund's case (c), the well depth of the same state for F–Xe has a more prominent molecular character, being confined in Hund's case (a) at the distances around the minimum. In Fig. 14 the well regions of the ground state of the three sys-

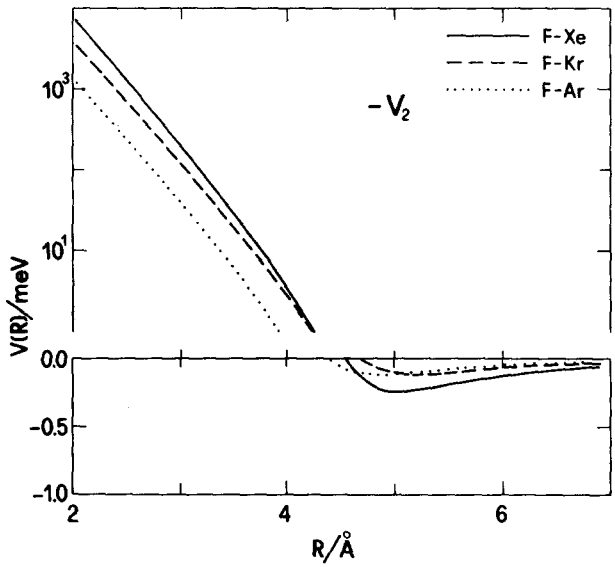

FIG. 11. Anisotropic interactions V_2 as a function of interatomic distances, plotted as $-V_2$ to stress similarities to an interatomic potential.

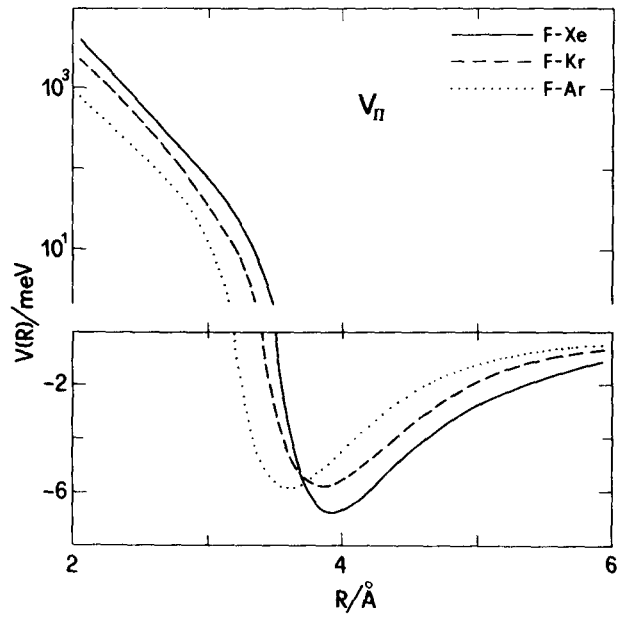

FIG. 13. V_Π interactions as a function of interatomic distances.

tems and their reduced forms [see, e.g., Eq. (12a)] are compared. Differences in their behavior are essentially due to the different role of the V_2 terms relative to V_0 and Δ. The larger differences between the reduced form of these interactions are found at distances where the changes between the Hund's case (c) and Hund's case (a) occur. These characteristic distances are reported in Table V.

Also shown in Table V are the values at the maximum of the **P** matrix elements. These nonadiabatic coupling terms are useful to estimate nonadiabatic effects and are needed to compute intramultiplet mixing, and orientation and alignment cross sections. In particular, since the first order nonadiabatic correction to adiabatic curves derived above is $(\hbar^2/2\mu)P^2$, we can easily verify from the values in Table V that this correction is small for all systems considered here.

VII. CONCLUDING REMARKS

The combined analysis of the experiments reported here and of those from other laboratories[3,5] has lead to potential functions $V_0(R)$ and $V_2(R)$ which fully characterize the weak forces which bind the diatomic molecules ArF, KrF, and XeF. Adiabatic curves for the ground and the first two electronic excited states have also been obtained and nonadiabatic coupling matrix elements clearly indicate the angu-

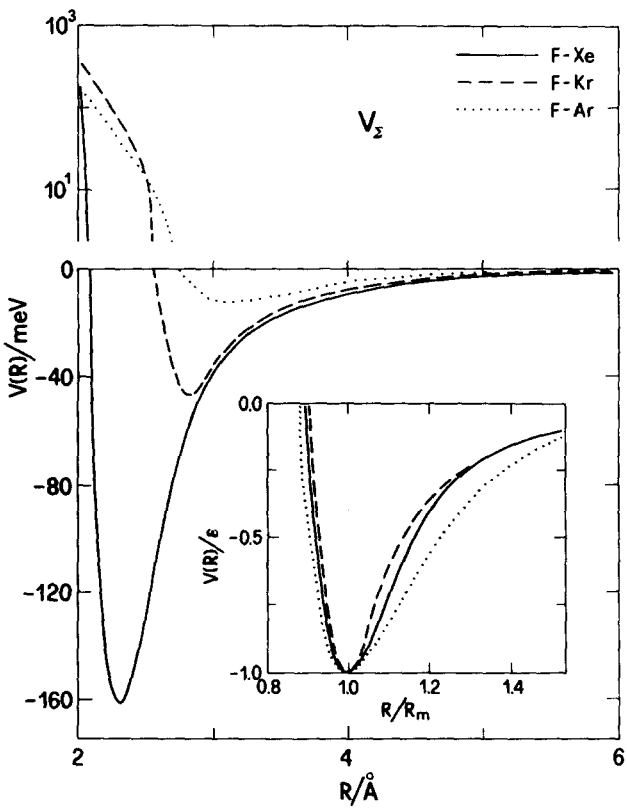

FIG. 12. V_Σ interactions as a function of interatomic distances. In the inset the reduced forms of the interactions are shown for comparison.

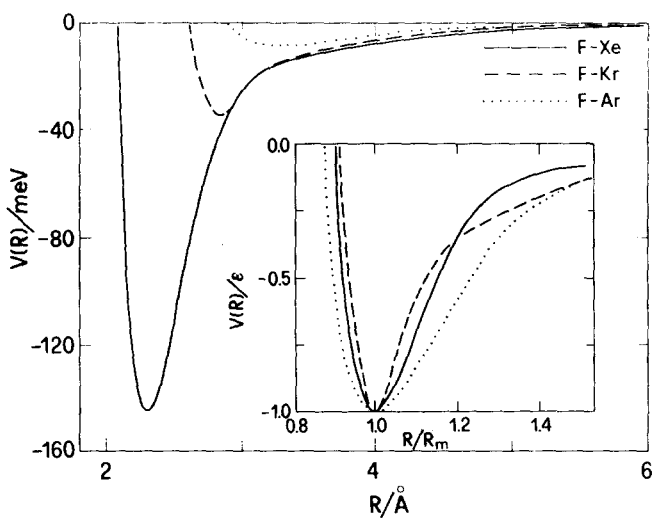

FIG. 14. Ground states $V_{|3/2\,1/2\rangle}$. In the inset the reduced forms of the interactions are shown for comparison.

TABLE V. Maxima in nonadiabatic coupling matrix elements: distances R_{max} and values P_{max}.

	F–Ar	F–Kr	F–Xe
$R_{max}/\text{Å}$	2.80	3.10	3.25
R_{max}/R_m[a]	0.85	1.09	1.40
$P_{max}/\text{Å}^{-1}$	0.64	0.64	0.67

[a] The R_m values are for the ground states, $V_{|3/2\,1/2\rangle}$.

lar momentum coupling schemes valid for these molecules in the well regions.

Trends in $V_0(R)$, the spherical part of the interaction, confirm what is presently known on the regularities in van der Waals forces[32]: With respect to the interactions of rare gases with oxygen,[8] an atom more polarizable than fluorine, spherical interactions V_0 are here seen to be weaker and to have a shorter range. Much less is known on anisotropies in the van der Waals region. The $V_2(R)$ functions obtained here and in the related work on other systems[8,33] provide useful information for the full understanding of weak interactions involving open shell atoms: When a comparison is made between the fluorine systems and those involving oxygen atoms,[8] it is observed that anisotropies in the present case decay faster, because of the smaller size of fluorine, but are stronger at short range presumably because of higher contributions from excited ionic states.

ACKNOWLEDGMENTS

Special thanks go to C. H. Becker, P. Casavecchia, and Y. T. Lee for extensive discussions on the Berkeley experiments, and to P. Toennies and K. Müller for providing detailed information on the Göttingen experiments. We acknowledge the help by P. Casavecchia, R. Candori, and F. Vecchiocattivi on several aspects of this work. This work has been supported by grants from the Italian Ministero della Pubblica Istruzione and from the Italian Consiglio Nazionale delle Ricerche.

[1] (a) J. Tellinghuisen, A. K. Hays, J. M. Hoffman, and G. C. Tisone, J. Chem. Phys. **65**, 4473 (1976); (b) J. Tellinghuisen, P. C. Tellinghuisen, G. C. Tisone, J. M. Hoffman, and A. K. Hays, *ibid.* **68**, 5177 (1978); (c) P. C. Tellinghuisen, J. Tellinghuisen, J. A. Coxon, J. E. Velazco, and D. W. Setser, *ibid.* **68**, 5187 (1978).

[2] J. H. Kolts, D. W. Setser, J. Phys. Chem. **82**, 1767 (1978); Y. C. Yu, D. W. Setser, and H. Horlguchi, *ibid.* **87**, 2199 (1983), and references therein; H. Helm, L. E. Jusinski, D. C. Lorents, and D. L. Huestis, J. Chem. Phys. **80**, 1796 (1984).

[3] (a) C. H. Becker, P. Casavecchia, and Y. T. Lee, J. Chem. Phys. **69**, 2377 (1978); (b) **70**, 2986 (1979).

[4] P. Casavecchia, G. He, R. K. Sparks, and Y. T. Lee, J. Chem. Phys. **77**, 1878 (1982), and references therein.

[5] K. Müller, Dissertation, Max-Planck Institute Fur Strömungsforschung, 1984.

[6] V. Aquilanti, E. Luzzatti, F. Pirani, and G. G. Volpi, Chem. Phys. Lett. **90**, 382 (1982). The analysis for XeF presented in this reference is here refined to include results of Refs. 3 and 5.

[7] M. Krauss and B. Liu, Chem. Phys. Lett. **44**, 257 (1976); P. J. Hay and T. H. Dunning, Jr., J. Chem. Phys. **66**, 1306 (1977); M. Krauss, *ibid.* **67**, 1712 (1977); T. H. Dunning, Jr. and P. J. Hay, *ibid.* **69**, 134 (1978); P. J. Hay, W. R. Wadt, and T. H. Dunning, Jr., Annu. Rev. Phys. Chem. **30**, 311 (1979), and references therein; M. Krauss, W. J. Stevens, and P. S. Julienne, J. Comput. Chem. **3**, 372 (1982).

[8] V. Aquilanti, R. Candori, and F. Pirani, J. Chem. Phys. **89**, 6157 (1988).

[9] C. H. Becker, P. Casavecchia, Y. T. Lee, R. E. Olson, and W. A. Lester, Jr., J. Chem. Phys. **70**, 5477 (1979).

[10] V. Aquilanti and G. Grossi, J. Chem. Phys. **73**, 1165 (1980).

[11] V. Aquilanti, P. Casavecchia, G. Grossi, and A. Laganà, J. Chem. Phys. **73**, 1173 (1980).

[12] V. Aquilanti, G. Grossi, and A. Laganà, Nuovo Cimento B **63**, 7 (1981).

[13] V. Aquilanti and F. Vecchiocattivi (to be published).

[14] (a) V. Aquilanti, G. Liuti, F. Vecchiocattivi, and G. G. Volpi, Chem. Phys. Lett. **15**, 305 (1972); (b) F. Pirani and F. Vecchiocattivi, J. Chem. Phys. **66**, 372 (1977); (c) E. Luzzatti, F. Pirani, and F. Vecchiocattivi, Mol. Phys. **34**, 1279 (1977); (d) B. Brunetti, F. Pirani, F. Vecchiocattivi, and E. Luzzatti, Chem. Phys. Lett. **55**, 565 (1978); (e) **58**, 504 (1978); (f) B. Brunetti, R. Cambi, F. Pirani, F. Vecchiocattivi, and M. Tomassini, Chem. Phys. **42**, 397 (1979); (g) B. Brunetti, G. Liuti, E. Luzzatti, F. Pirani, and F. Vecchiocattivi, J. Chem. Phys. **74**, 6734 (1981); (h) V. Aquilanti, R. Candori, E. Luzzatti, F. Pirani, and G. G. Volpi, *ibid.* **85**, 5377 (1986).

[15] V. Aquilanti, F. Pirani, E. Luzzatti, and G. G. Volpi, Gazz. Chim. Ital. **110**, 57 (1980).

[16] B. Brunetti, G. Liuti, F. Pirani, and E. Luzzatti, Chem. Phys. Lett. **84**, 201 (1981).

[17] (a) V. Aquilanti, G. Liuti, F. Pirani, F. Vecchiocattivi, and G. G. Volpi, J. Chem. Phys. **65**, 4751 (1976); (b) V. Aquilanti, E. Luzzatti, F. Pirani, and G. G. Volpi, *ibid.* **73**, 1181 (1980).

[18] T. Nenner, H. Tien, and J. B. Fenn, J. Chem. Phys. **63**, 5349 (1975); **64**, 3902 (1976); see also Ref. 14(b).

[19] (a) N. F. Ramsey, *Molecular Beams* (Clarendon, Oxford, 1956); (b) K. Berkling, Ch. Schlier, and P. Toschek, Z. Phys. **168**, 81 (1962); (c) M. A. D. Fluendy and K. P. Lawley, *Chemical Applications of Molecular Beams Scattering* (Chapman and Hall, London, 1973); (d) H. Hishinuma and O. Sueoka, Chem. Phys. Lett. **98**, 414 (1983); **121**, 293 (1985); (e) J. Reuss, *Atomic and Molecular Beams Methods*, edited by G. Scoles (Oxford, New York, 1987).

[20] This is true when as in the present case the deflection of the particle within the magnet is small with respect to the dimensions of the polar expansions. This is the condition for an essentially constant field gradient $\partial B/\partial z$ [see Ref. 19(a)].

[21] G. H. Fuller and V. W. Cohen, *Nuclear Data Tables*, edited by K. Way (Academic, New York, 1969).

[22] B. P. Straughan and S. Walker, *Spectroscopy* (Chapman and Hall, London, 1976), Vol. 1.

[23] A. R. Edmonds, *Angular Momentum in Quantum Mechanics* (Princeton University, Princeton, 1960).

[24] V. Aquilanti, G. Grossi, and F. Pirani, *Electronic and Atomic Collisions*, invited papers XIII ICPEAC, edited by J. Eichler, I. V. Hertel, and N. Stolterfoht (North-Holland, Berlin, 1983), p. 441.

[25] V. Aquilanti, F. Pirani, and F. Vecchiocattivi, *Structure and Dynamics of Weakly Bound Molecular Complexes*, edited by A. Weber (Plenum, New York, 1987), p. 423.

[26] R. H. G. Reid and D. Dalgarno, Phys. Rev. Lett. **22**, 1029 (1969); R. H. G. Reid, J. Phys. B **6**, 2018 (1973).

[27] F. Pirani and F. Vecchiocattivi, Mol. Phys. **45**, 1003 (1982).

[28] A preliminary analysis of the glory locations has been performed in terms of a single effective potential using a LJ(12,6) model to show trends and regularities in the van der Waals forces. That model was chosen for a consistent comparison with other systems involving open shell atoms, such as nitrogen, which had been analyzed only in terms of such a simple model. The potential parameters so obtained were reported in Ref. 32.

[29] From H. J. Werner and W. Meyer, Phys. Rev. A **13**, 13 (1976), one has for the relative polarizability anisotropy of ground state fluorine atom, $(\alpha_\Sigma - \alpha_\Pi)/(\alpha_\Sigma + 2\alpha_\Pi) \simeq -0.09$. From the Slater–Kirkwood approximation [J. C. Slater and J. G. Kirkwood, Phys. Rev. **37**, 682 (1931)] this leads to $C_2/C_0 \simeq 0.12$, where C_2 is the long range R^{-6} anisotropic component [see Eq. (13)]. This value has been used for all systems.

[30] G. Liuti, E. Luzzatti, F. Pirani, and G. G. Volpi, Chem. Phys. Lett. **135**, 387 (1987).

[31] P. Casavecchia (private communication).

[32]G. Liuti and F. Pirani, Chem. Phys. Lett. **122**, 245 (1985), and references therein. In this paper a general correlation in terms of polarizability is given, which allows reasonable estimates of ϵ and R_m values for any interaction pair considered. These estimates agree with the ESMSV values from present analysis considering the overall uncertainties involved. For further details, see V. Aquilanti, G. Liuti, F. Pirani, and F. Vecchiocattivi, J. Chem. Soc. Faraday 2 (in press).

[33]V. Aquilanti, R. Candori, L. Mariani, F. Pirani, and G. Liuti, J. Phys. Chem. (in press).